RSC Advances

PAPER

View Article Online
View Journal | View Issue



Cite this: *RSC Adv.*, 2021, **11**, 10285

# Highly sensitive and rapid responding humidity sensors based on silver catalyzed $Ag_2S$–$TiO_2$ quantum dots prepared by SILAR

Zu-Yin Deng,[a] Ping-Chang Chiang,[a] Kuen-Lin Chen,[ab] Jau-Han Chen[c] and Chiu-Hsien Wu*[ab]

We developed a resistive humidity sensor based on a heterojunction of silver sulfide ($Ag_2S$) quantum dots (QDs) and $TiO_2$ because of its specificity to water vapor adsorption and its insensitivity to environmental gases. The QDs were grown on a mesoporous $TiO_2$ layer using the successive ionic layer adsorption and reaction (SILAR) method. The boundary condition between $TiO_2$ and $Ag_2S$ provides a tunable energy gap by adjusting the number of SILAR cycles. Besides, the large surface-to-volume ratio of QDs provides a strong water vapor adsorption ability and electron transfer. Nano-silver precipitated during the SILAR process provides free electrons and lowers the Fermi level to between n-type $TiO_2$ and p-type $Ag_2S$. The resistance response increased significantly to 4600 and the reaction equilibrium time decreased greatly to 7 seconds due to the presence of nano-silver. Finally, the $Ag_2S$ QDs possess a best sensing range of 13–90%. To sum up, $Ag_2S$ QDs are high sensitivity and selectivity humidity sensors.

Received 17th November 2020
Accepted 4th March 2021

DOI: 10.1039/d0ra09756j

rsc.li/rsc-advances



## 1. Introduction

Humidity sensors have been widely employed in various fields, including ecological, mineral processing, and food processing.[1–3] The moisture in the environment can cause oxidation reactions, which change the properties of materials. It may also cause problems such as bacterial growth and decomposition. Therefore, a fast-responding and high-sensitivity humidity sensor is useful for monitoring and regulating applications.

Humidity sensors can be classified into five different types: hygrometric, resistive, capacitive, gravimetric, and optical sensors. An example of a capacitive humidity sensor based on nano-gold is reported in ref. 4. A resistive sensor based on CA-NH4BF4-PEG600 thin-films responds to relative humidity (RH) due to proton transfer, known as the Grotthuss mechanism.[1,5] Gravimetric humidity sensors are based on piezoelectric PVDF polymer materials.[6] Most commercial humidity sensors are based on the capacitive method because of low power consumption and high output signals. However, resistive sensors also have numerous advantages such as low-cost, fast response, ease of mass production, easy of fabrication, and adjustable properties. Thus, they have significant potential for application as humidity sensors. Many previous reports used metal oxide resistive humidity sensors, such as $TiO_2$, $WO_3$, ZnO, and $Fe_2O_3$.[6,7] This type of material provides a stable detection range of about RH 20–80%

Heterogeneous junctions formed by composite different type materials can beneficial to the electron transfer. $Ag_2S$ is a p-type semiconductor with a low energy gap (~1.1 eV).[8,9] $Ag_2S$ nanowire have been reported based on photoswitches and room temperature oxygens sensors as ultralong single-crystalline.[10] Further, $TiO_2$@$Ag_2S$ has excellent chemical stability and electron transfer characteristics.[11] It was used in photovoltaic devices and solar cells due to its high mobility.[12] In recent years, numerous studies on QDs have been reported due to many advantages. Owing to their tunable energy gap, low-cost and simplicity of preparation, QDs are usually decorated with different materials, including thin-films, nanowires, and nanorods. Herein, method the particle size by adjusting the number of the successive ionic layer adsorption and reaction (SILAR) cycles. And consequently, the energy gap of the sample was adopted to control due to the quantum-size effect.[13,14] Compared to other synthesis methods, the SILAR method has several merits: (i) it provides a low-cost and convenient means for large area deposition on the substrate, (ii) vacuum and high-quality substrates are not required.[15,16]

In this study, we develop a semiconductor humidity sensor based on the $Ag_2S$–$TiO_2$ heterostructure. We develop SILAR methods to synthesize $Ag_2S$ QDs on a mesoporous $TiO_2$ layer to enhance the sensitivity and response rate. The sensing characteristics for different numbers of SILAR cycles was studied. At the same time, we study the repeatability and selectivity of the $Ag_2S$ QDs humidity sensors.

[a]*Department of Physics, National Chung Hsing University, Taichung 402, Taiwan. E-mail: chwu@phys.nchu.edu.tw; Fax: +886-4-2286253; Tel: +886-4-22840427*

[b]*Institute of Nano-Science, National Chung Hsing University, Taichung 402, Taiwan*

[c]*Department of Materials Science and Engineering, Da-Yeh University, Changhua 55, Taiwan*

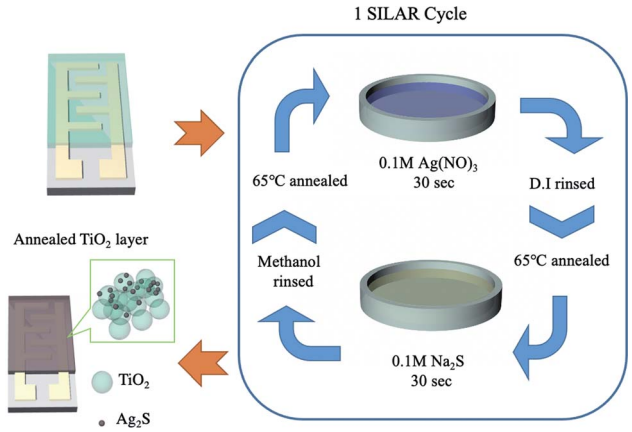


Fig. 1 Schematic of QD film process by SILAR method.

## 2. Experimental

### 2.1 Material preparation

A gel of 30 nm $TiO_2$ (Dyesol $TiO_2$ Paste DSL 30NR-D) is dissolved in ethanol (anhydrous 99.5 UP) solution (1 : 1.5 w/w), and was spin-coated on the surface of the finger electrode shown in Fig. 1. It was subsequently annealed at 500 °C for 15 min. Then, the substrate with $TiO_2$ was immersed in 0.1 M $Ag(NO)_3$ (Honeywell Fluka) solution for 30 seconds, rinsed with deionized water, and annealed at 65 °C. Next, the sample was immersed in 0.1 M $Na_2S$ (Acros Organics) solution for 30 seconds, to allow a replacement reaction with sulfur to occur. It was rinsed with methanol (Macron Fine Chemicals) and then annealed at 65 °C. These immersion steps were repeated for 4–12 cycles. Finally, the samples were annealed at 400 °C for 10 min in a nitrogen environment.

### 2.2 Humidity sensing device setup

Humidity was measured in a chamber. Water vapor was provided by a vapor-generator and was exhausted by using a pump. The reference gases including oxygen, carbon-monooxide and nitrous oxide was from gas cylinders. The entire experiment was carried out at room temperature (25 ± 1.5 °C). The resistance of the sensing device was measured by a high resistance meter (HP4349A) and the reference humidity was monitored by a commercial capacitive humidity sensor (DHT22). The material properties of $Ag_2S$ were measured by a UV-visible spectrometer (Jasco-V-550), X-ray diffractometer (XRD, Bruker d8SSS, Cu K$\alpha$1), and transmission electron microscopy (TEM, Jeol JEM-2010).

## 3. Results and discussion

The UV-Vis spectrum of $TiO_2$ and six $Ag_2S/TiO_2$ samples with different numbers of successive ionic layer adsorption and reaction (SILAR) cycles are shown in Fig. 2(a). The absorption intensity was increases depends on the cycles increasing. The cycle number; thus, it with. The absorption rate is depicted in the Tauc plot. The calculated energy gaps ($E_g$) for 4, 6, 7, 8, 9, and 12 cycle samples are 2.1, 1.9, 1.6, 1.5, 1.4, and 1.3 eV, respectively (Fig. 2(b)). The energy gap increased due to the quantum size effect, and the particle size gradually increases because of the reduction reaction and deposition in SILAR step.[14]

XRD was used to determine the phases of crystals and crystallite size. The XRD spectra of $TiO_2$ layers and $Ag_2S$ quantum dots (QDs) are shown in Fig. 3(a). The XRD spectra of $Ag_2S$, Ag and $TiO_2$ are in perfect accordance with JCPDS 00-001-1151, 01-087-0717 and 01-086-1157, respectively. Crystallite sizes were calculated by the semi-empirical Debye–Scherrer formula.

$$D = \frac{K\lambda}{\beta \cos \theta} \quad (1)$$

where $D$ is the crystallite size, $K$ is a crystallite shape factor approximated as 0.9, $\lambda$ is the X-ray wavelength (Cu K$\alpha$1 ≅ 1.5418 Å), β is the full-width at half-maximum (FWHM), and $\theta$ is the Bragg angle (in radians). Thus, the crystallite size is calculated to be 19.25 nm. The surface morphology and the nanostructure could be easily observed from the TEM image, and consequently the particle size and inter-planar spacing were obtained. Fig. 3(b and c) demonstrates that the $Ag_2S$ QD particle sizes are approximately 15 nm, which corresponds to the crystallite sizes obtained from the Debye–Scherrer formula. Besides, $Ag_2S$ QDs are attached to $TiO_2$. The lattice spacing of $Ag_2S$ is 0.34 nm,

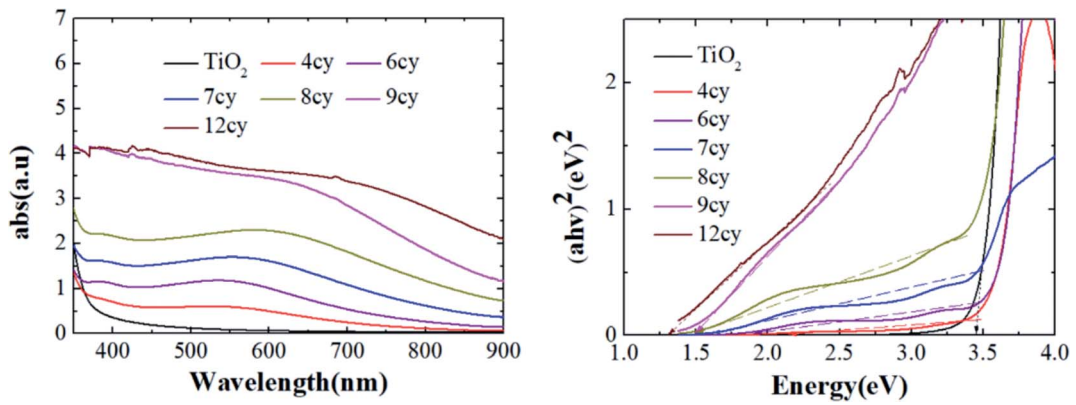


Fig. 2 Absorption spectrum of QD film (a) UV-Vis spectrum and (b) Tauc-plot.

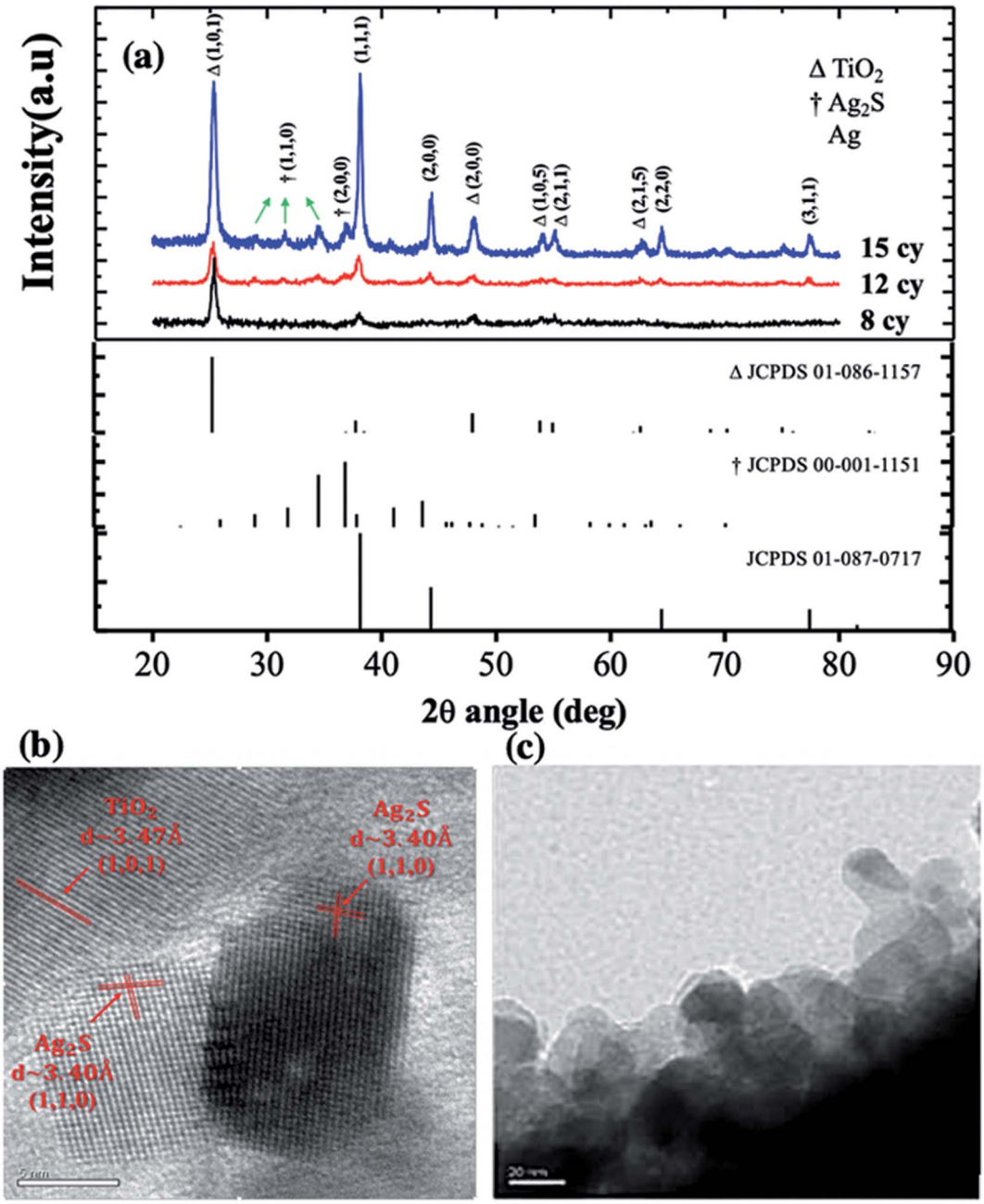


Fig. 3 Material characteristics of QD film (a) XRD spectra (b) and (c)TEM images.

while the crystal planes correspond to the (1,1,0) facet, which corresponds to JCPDS 00-002-0998.

The $Ag_2S$ QDs have a high response to $H_2O$ molecules in the atmosphere. The ·OH was dissociated from $H_2O$ and absorbed on positively charged Ag atoms following eqn (2). This provides more free electrons to $TiO_2$ shrinking the depletion and decreasing the overall resistance of the material.

$$Ag_2S(h^+) + H_2O \rightarrow Ag_2S + H^+ + \cdot OH \quad (2)$$

Fig. 4 exhibits the resistance response to relative humidity (RH) of 8-cycle $Ag_2S$, which was considered to have the broadest sensing range of 13–90% RH. The lowest measured humidity of 13% corresponds to $1.6 \times 10^{10}$ Ω which decreased to $6.8 \times 10^6$ Ω at 90% RH. The resistance response, as defined by eqn (3), was approximately 4600.

$$\text{Response} = \frac{R_L - R_H}{R_H} \quad (3)$$

where $R_L$ is the sample resistance at low RH and $R_H$ that at high RH.

The $TiO_2$ film coated on substrate has response between RH 20–85%, the response was 423, with the response/recovery time ~50/100 s. Of all SILAR depositions performed in this

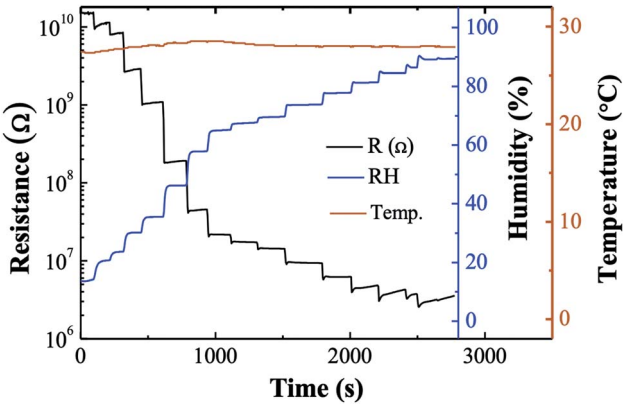


Fig. 4 Resistance measurement under 13–90% RH (8-cycle sample).

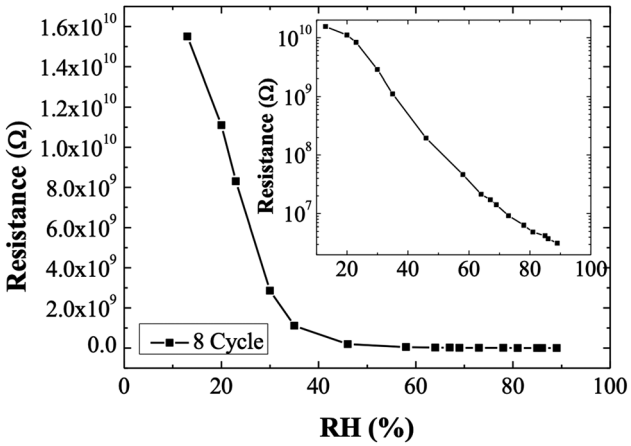


Fig. 6 Fitting curve of resistance to RH%. Insert is plot of log *R* to RH%.

experiment, the 5-cycle sample had the highest resistance. The measurement range was RH 30–85% (Fig. 5), and the resistance varied over the range $3 \times 10^{10}$ to $1 \times 10^{7}$ Ω. However, this sample has poor stability at high humidity. The resistance value gradually increases when the RH exceeds 88%. Despite adsorbed steam still causing the resistance to change, the increasing baseline caused a loss of correspondence between humidity and resistance. As the numbers of SILAR cycles increases, the problem of instability was gradually ameliorated. The sensing range of the 4-cycle sample was smaller than that of the 5-cycle sample under low RH. This might be regarded as being due to a smaller concentration of $Ag_2S$. On the other hand, smaller QDs have a larger energy gap, hence the difficulty of electron migration is increased. For this reason, the low-cycle samples provide higher response, but poor stability.

The measurement range decreased gradually for more than 8-cycles. The range of the 9-cycle sample is merely RH 46–88%. The Fermi-level is reduced as the particle size increases. This improves electron transport and reduces resistance. Since there are more free electrons, the low humidity cannot be identified by resistance change. For the same reason, the 12-cycle sample has an even worse response (RH 55–82%).

Fig. 6 shows the correlation between humidity (RH) and resistance ($R$) of the 8-cycle sample. For the range RH 13–90%, the response trend is clearly divided into two regions. The resistance increases linearly and significantly relative to the humidity decreases over the range 13–30% RH. The linear equation was $R = -7.49 \times 10^{8}RH + 2.55 \times 10^{10}$. The resistance change up to 14 gigaohms and provided an accurate RH measurement. Further, this sample has good humidity dependence over the range 30–90% RH. According to eqn (2), the water vapor adsorption and dissociation reduces the number of $Ag_2S$ holes and decreases the resistance. The conductivity is proportional to the free electrons obtained by $Ag_2S$ from $H_2O$.[20] The RH range between 20–90% $Ag_2S$ QDs and $H_2O$ have a high response (~1000). The high reaction rate is due to the large surface area of the QDs. The QDs provide a large number of carriers to react with $H_2O$.

The 8-cycle sample resistance was measured for three consecutive humidity cycles of the same RH values as shown in Fig. 7. The sample exhibited a stable resistance value over the range 13–90% RH. According to the first derivative of the resistance, the $Ag_2S$ sample presents an instantaneous response and recovery times of 7 and 19 seconds respectively (Fig. 7). In

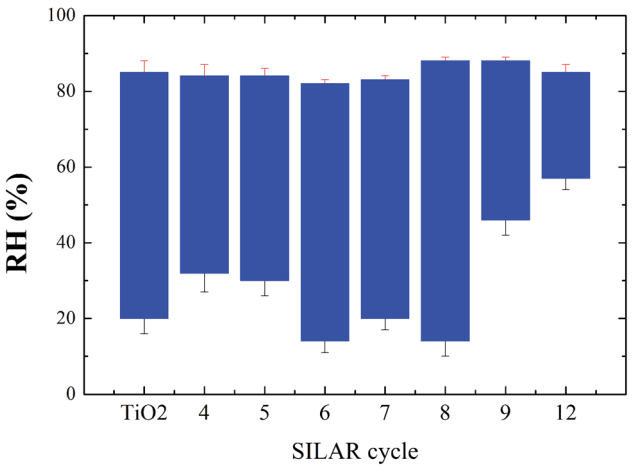


Fig. 5 Sensing range comparison samples with different SILAR cycles.

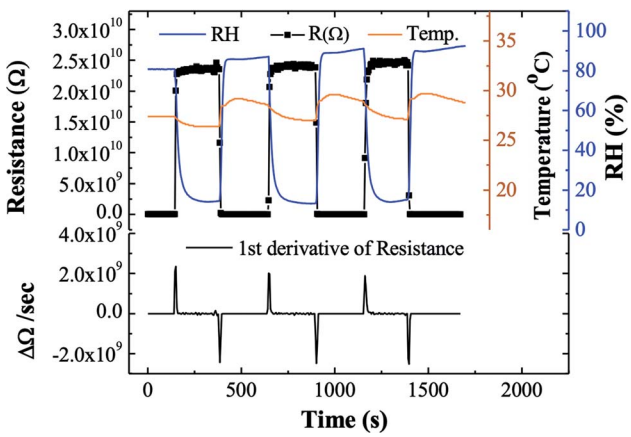


Fig. 7 Sensor stability and repeatability. The measure range was 13–90%.

Table 1 Simple comparison between $Ag_2S$ QDs and reported humidity sensors

| Sensor classification | Sensing material | Range (% RH) | Sensitivity (1% RH) | Response | Response/recovery time(s) | Ref. |
|---|---|---|---|---|---|---|
| Resistive | $Ag_2S$ | 13–90 | 195.3MΩ | 4600 | 7.23/19.03 | This work |
| Capacitive | Au-PVA | 11.3–93 | 0.05 nF | 0.53 | 113–188/53–94 | 4 |
| Resistive | Cellulose acetate-CuO | 0–90 | 3.8 MΩ | 1093 | 13/17 | 17 |
| Gravimetric | CNCs | 11.3–97.3 | 55.3/275Hz | 1.28 | 60/15 | 18 |
| Piezoresistive | ZnO NRs | 30–80 | 3.35–15 Hz | — | 46/167 | 19 |

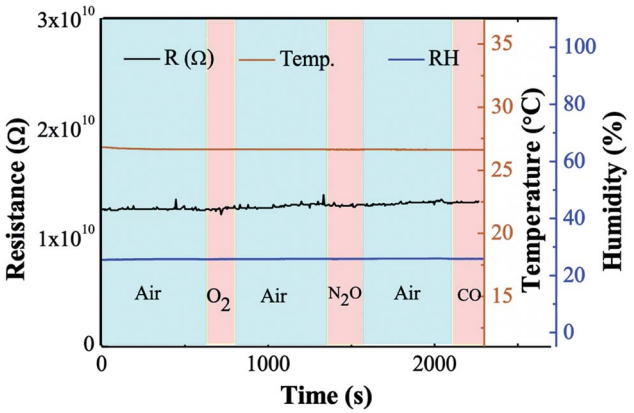


Fig. 8 The ambient gas selectivity of $Ag_2S$@$TiO_2$ samples.

comparison to the recently reported humidity sensors of different types listed in Table 1, the proposed $Ag_2S$ QDs possess a high response and fast response/recovery time. Thus, $Ag_2S$ QDs are well-suited to humidity sensors.

In order to observe the effect of ambient gases, several arid gases from cylinder were pumped into the chamber, including oxygen, carbon monoxide (reducing gas) and nitrous oxide gas (oxidizing gas) (Fig. 8). The humidity was fixed at 26% RH. The resistance has no response to gases with different electron affinity which ensured this sample was stable and unaffected by the ambient gas.

The ·OH from the water vapor was oxidized on the surface of $Ag_2S$, hence providing free electrons. According to the catalytic literature of $TiO_2$@$Ag_2S$, the coexistence of Ag and $Ag_2S$ can further enhance the transfer of electrons (Fig. 9a).[21–23] $TiO_2$ is an n-type material with a wide energy gap. On the other hand, $Ag_2S$ is a p-type material with wide energy gap which provides reaction sites. Compared with NHE, the conduction band of $TiO_2$ was 0.8 eV higher than the valence band of $Ag_2S$. This energy gap can be adjusted by adjusting the number of SILAR cycles. The smaller the energy gap is, the more efficient electron transfer is. The presence of silver particles lowers the Fermi-level, which increase electron transfer (Fig. 9b). Therefore, in our experiment, the 8-cycle SILAR sample exhibits the best humidity sensing range of 13–90% RH. Furthermore, the response time of the absorption process due to the catalysis of silver particles is barely seven seconds. To verify the contributions of silver particles to the RH measurement, the dipping time of sodium sulfide solution was increased from 30 s to 90 s and thus more $Ag_2S$ were synthesized from Ag particles. There was a significant decrease of absorption peak of Ag particles in UV-Vis spectrum. The resistance response were reduced to 39. Besides, the response time also increased significantly. This result confirms that the silver particles have a catalytic effect which contribute to the humidity sensing.

## 4. Conclusion

In this experiment, chemical methods were used to synthesize $TiO_2$@$Ag_2S$ quantum dots (QDs), and the 8-cycle sample

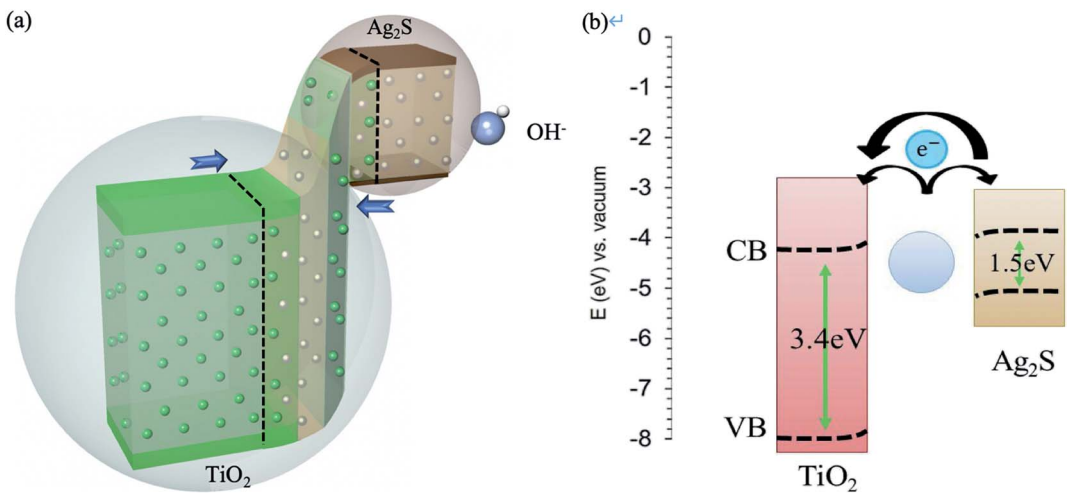


Fig. 9 Diagram of electron-transfer mechanism. (a) Electron transfer of $OH^-$ adsorption (b) catalysis of silver particles.

achieved the highest sensing range of 13% to 90%. The energy gap of was tuned to 1.5 eV based on the quantum-size effect of $Ag_2S$. Owing to the catalytic effect of metallic silver, it provides a high resistance-based response of 4600, an accuracy of 1% RH, and high reaction speed. The $Ag_2S$ QDs has the features of uninfluenced by environmental pollutants and reproducibility. Therefore, $Ag_2S$ QDs have high practical value as a humidity sensor owing to its high efficiency and simple-operation.

## Conflicts of interest

There are no conflicts to declare.

## Acknowledgements

The authors thank the financial supports of the Ministry of Science and Technology of Taiwan (MOST 108-2112-M-005-001, MOST 109-2112-M-005-007).

## References

1 H. Farahani, R. Wagiran and M. N. Hamidon, *Sensors*, 2014, **14**(5), 7881–7939.
2 A. Tripathy, S. Pramanik, J. Cho, J. Santhosh and N. A. A. Osman, *Sensors*, 2014, **14**(9), 16343–16422.
3 Z. Chen and C. Lu, *Sens. Lett.*, 2005, **3**(4), 274–295.
4 W. Yao, X. Chen and J. Zhang, *Sens. Actuators, B*, 2010, **145**(1), 327–333.
5 N. I. Harun, R. M. Ali, A. M. M. Ali and M. Z. A. Yahy, *Phys. Procedia*, 2012, **25**, 221–226.
6 A. Glück, W. Halder, G. Lindner, H. Müller and P. Weindler, *Sens. Actuators, B*, 1994, **19**(1–3), 554–557.
7 P. V. Shinde, S. Gagare, C. S. Rout and D. J. Late, *RSC Adv.*, 2020, **10**(49), 29378–29384.
8 F. Jiang, Q. Tian, M. Tang, Z. Chen, J. Yang and J. Hu, *CrystEngComm*, 2011, **13**(24), 7189–7193.
9 H. Dlala, M. Amlouk, S. Belgacem, P. Girard and D. Barjon, *Eur. Phys. J.: Appl. Phys.*, 1998, **2**(1), 13–16.
10 D. Wang, C. Hao, W. Zheng, Q. Peng, T. Wang, Z. Liao, D. Yu and Y. Li, *Adv. Mater.*, 2008, **20**(13), 2628–2632.
11 W. P. Lim, Z. Zhang, H. Y. Low and W. S. Chin, *Angew. Chem., Int. Ed.*, 2004, **43**(42), 5685–5689.
12 Y. Xie, S. H. Yoo, C. Chen and S. O. Cho, *Mater. Sci. Eng., B*, 2012, **177**(1), 106–111.
13 D. Yan, Y. He, Y. Ge and G. Song, *Sens. Actuators, B*, 2017, **240**, 863–869.
14 A. I. Ekimov, Al. L. Efros and A. A. Onushchenko, *Solid State Commun.*, 1985, **56**(11), 921–924.
15 H. M. Pathan and C. D. Lokhande, *Bull. Mater. Sci.*, 2004, **27**(2), 85–111.
16 S. I. Sadovnikov and E. Y. Gerasimov, *Nanoscale Adv.*, 2019, **1**(4), 1581–1588.
17 M. T. S. Chani, K. S. Karimov, S. B. Khan and A. M. Asiri, *Sens. Actuators, A*, 2016, **246**, 58–65.
18 Y. Yao, X. H. Huang, B. Y. Zhang, Z. Zhang, D. Hou and Z. K. Zhou, *Sens. Actuators, B*, 2020, **302**, 127192.
19 J. Xu, M. Bertke, X. Li, H. Mu, H. Zhou, F. Yu, G. Hamdana, A. Schmidt, H. Bremers and E. Peiner, *Sens. Actuators, B*, 2018, **273**, 276–287.
20 A. K. Kralj, *J. Ind. Eng. Chem.*, 2007, **13**(4), 631–636.
21 H. Yu, W. Liu, X. Wang and F. Wang, *Appl. Catal., B*, 2018, **225**, 415–423.
22 A. Badawi, *Phys. E*, 2019, **109**, 107–113.
23 W. L. Ong, Y. F. Lim, J. L. T. Ong and G. W. Ho, *J. Mater. Chem. A*, 2015, **3**(12), 6509–6516.